IEEE Access
Multidisciplinary | Rapid Review | Open Access Journal

Received July 14, 2020, accepted July 27, 2020, date of publication August 3, 2020, date of current version August 14, 2020.

Digital Object Identifier 10.1109/ACCESS.2020.3013605

Feasibility of Plasmonic Circuits in Nanophotonics

MITSUO FUKUDA, (Member, IEEE), SHINYA OKAHISA, YUTA TONOOKA, MASASHI OTA, (Member, IEEE), TAKUMA AIHARA, (Member, IEEE), AND YASUHIKO ISHIKAWA, (Member, IEEE)

Department of Electrical and Electronic Information Engineering, Toyohashi University of Technology, Toyohashi 441-8580, Japan

Corresponding author: Mitsuo Fukuda (fukuda@ee.tut.ac.jp)

This work was supported in part by the Japan Society for the Promotion of Science (JSPS) KAKENHI under Grant JP26289103, Grant JP25630147, Grant JP16K14253, and Grant JP18K04282.

ABSTRACT The configuration of plasmonic circuits comprising SiO_2-load waveguides and their characteristics within the nanophotonic range are presented and compared with electronic and lightwave circuits in 1300 and 1550 nm wavelength bands. In the nanophotonic range of less than 1 μm, plasmonic signals propagate in narrow waveguides with cross-sections less than a few hundred square nanometers, while lightwaves exhibit only slight propagation in high-refractive-index (i.e., Si) waveguides owing to the transmission loss increase via the cut-off wavelength of the waveguide. Additionally, the plasmonic signal transmission loss is lower than that of electric signals for transmission lengths less than a few hundred micrometers. During signal transmission, a narrow spectral width of the plasmonic signals is needed to suppress any signal shape deformation induced by the frequency dependence of the collective oscillation of electrons in plasmonic signals. In the nanophotonic range, the degree of integration for plasmonic circuits is not governed by the transmission loss but by the leak distance of the plasmonic signal optical field from the side-walls of the waveguides and components. Employing a metal/insulator/metal structure in plasmonic circuits is a valid way to heighten the integration density, and its effectiveness is numerically and experimentally confirmed in a plasmonic multiplexer less than 1 μm in length. On the basis of these results, the feasibility of plasmonic circuits is discussed and it can be said that plasmonic circuits including waveguides and components are promising photonic techniques for signal transmission in the nanophotonic range.

INDEX TERMS Integrated circuit, integrated optics, integrated optoelectronics, nanophotonics, optical interconnection, plasmonics, surface plasmon polariton, wavelength division multiplexing.

I. INTRODUCTION

Photonics has historically been used to support daily life of our society, and the techniques in the field are indispensable for constructing and maintaining societal infrastructure. These techniques require key photonic components whose scale and power consumption requirements are being reduced as technology advances. Recently, optical interconnects have begun to be used in silicon integrated circuits (ICs) to enhance the information processing speed and catch up with the explosive increase in information demand. The lightwave circuits of interconnects typically comprise silicon waveguides that possess a relatively high refractive index. In the range of less than sub-wavelength optics, however, photonic crystals and high-refractive-index waveguides using lightwaves as signals are physically difficult to apply to circuits [1].

At such small scales, surface plasmon polariton (SPP) waveguides are effective for constructing nanophotonic circuits. Various kinds of plasmonic waveguides have been developed and reported, such as index waveguides [2]–[5], grooved waveguides [6], [7], hybrid waveguides [8]–[10], and metal/insulator/metal (MIM) structured waveguides [11]–[16]. These various waveguides have different signal transmission performance characteristics [17], [18]. Grooved, hybrid, and MIM waveguides can be easily constructed in the range of less than 100 nm (i.e., nanophotonics range), and Mach-Zehnder and ring resonators have also been fabricated using those waveguides. The construction of multiplexers and demultiplexers for wavelength-division multiplexing (WDM) techniques is, however, easier for

The associate editor coordinating the review of this manuscript and approving it for publication was Leo Spiekman.

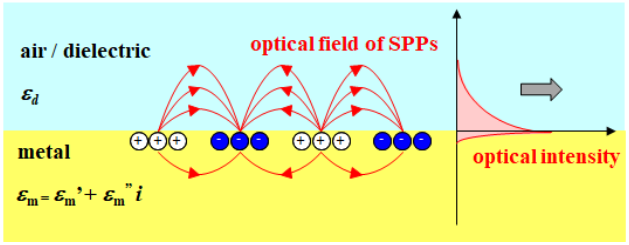

FIGURE 1. Schematic of SPPs at the interface between metal and air/dielectric.

MIM waveguides than the other waveguides because of the difficulty of transmission mode controls using multimode waveguides in the latter cases.

The waveguides comprising dielectric stripes deposited on a metal film (i.e., dielectric-loaded surface plasmon (DLSP) waveguides) are technically simple and are easy to translate to waveguide devices and to integrate with silicon ICs. These design and fabrication techniques can be easily expanded to MIM waveguides and other functional structures. The MIM waveguides are particularly attractive for constructing plasmonic components, although their structures are slightly complicated. Therefore, we have developed plasmonic components and circuits using waveguides consisting of a SiO_2 stripe on a metal film and MIM waveguides [19].

In this article, the feasibility of plasmonic circuits based on the DLSP and MIM waveguides are discussed for nanoscale application. The materials used in the plasmonic circuits are discussed in Sec. II. The scale of the plasmonic circuits is discussed relative to other circuits in Sec. III, and the characteristics required for signal transmission in the circuits are discussed in Sec. IV. The signal transmission performances in the plasmonic waveguides are presented relative to those of electric and lightwave circuits in Sec. V. The application areas for plasmonic circuits are discussed in Sec. VI. The results obtained are summarized in Sec. VII.

II. METALS FOR PLASMONIC CIRCUITS

The SPPs are electromagnetic waves that propagate along a conductor surface at the speed of light, and represent collective oscillations of electrons coupled with the optical field at the nanoscale beyond the diffraction limit of propagating lightwaves (Fig.1). To construct plasmonic components, waveguides, and circuits, metals with low electric resistivity are required because the losses during signal transmission are primarily caused by ohmic loss. (The phenomena of generating SPPs in metal have been comprehensively explained in Ref. [20].) The ohmic loss of SPPs is mainly owing to a disturbance of the collective oscillation of electrons by the electric resistance induced by electron collisions and scattering via impurities, defects, and phonons in the metal. From the viewpoint of low electric resistivity, metals such as Al, Cu, Ag, and Au are popular, and Al and Cu are typically used in silicon ICs.

For the metals popular in plasmonic circuits such as Al, Cu, Ag, and Au, the propagation lengths (i.e., inverse of

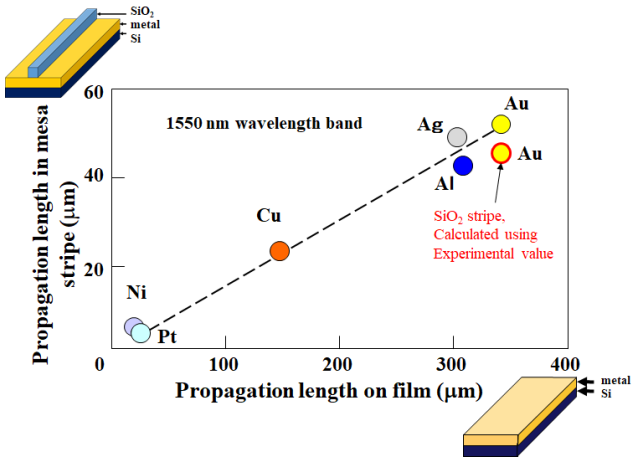

FIGURE 2. Calculated propagation length of SPPs on metal films and in the SiO_2 mesa structure.

loss coefficients) were calculated with the three-dimensional finite-difference time-domain (3D-FDTD) method using electromagnetic wave analysis software (Pointing for Optics, Fujitsu). The propagation length, d_p, is expressed by the next equation,

$$d_p = 1/2k'', \tag{1}$$

where k'' is the imaginary part of the SPP wavenumber k which is given by the dispersion relation

$$k = (\omega/c)[\varepsilon_d \varepsilon_m/(\varepsilon_d + \varepsilon_m)]^{1/2}, \tag{2}$$

where ω is the SPP angular frequency; c is the speed of light; and ε_d and ε_m are the dielectric constants of the dielectric substance (or air) and the metal, respectively. Using Eq.(1), the propagation length for a SiO_2 (refractive index: 1.45) mesa stripe waveguide [500 nm (thickness, T)× 500 nm (width, W)] on various metal films and metal surfaces were calculated in the 1550 nm wavelength band and are shown in Fig.2. Here, the complex refractive indices of metals presented in Ref. [21] (e.g., $0.56 + 11.5i$ (Au), $0.51 + 10.8i$ (Ag), $1.44 + 16.0i$ (Al), $0.61 + 8.3i$ (Cu), $5.98 + 6.8i$ (Ni), $5.31 + 7.0i$ (Pt) in the 1550 nm wavelength band) were used for the calculations. For the SiO_2 mesa structure on a Au film, an experimentally-obtained value is also plotted. The propagation length is shorter in the SiO_2 mesa structure when compared with the case on the metal film because the waveguide is etched down to the SiO_2 mesa structure, increasing the scattering loss at the side-wall. The propagation length of Cu is much smaller than that of Au, Ag, and Al.

The transmission loss is not solely determined by the electric resistivity. Fig.3 shows the SPP optical intensity distribution ratio between the metal and SiO_2/air for plasmonic waveguides composed of a SiO_2 stripe on various metal films. Also shown are cross-sectional views of the optical field calculated using the 3D-FDTD method. The penetration depth in Cu is relatively large, and thus the SiO_2 waveguide on Cu exhibits an increased loss and weaker optical field compared with that on other metals.

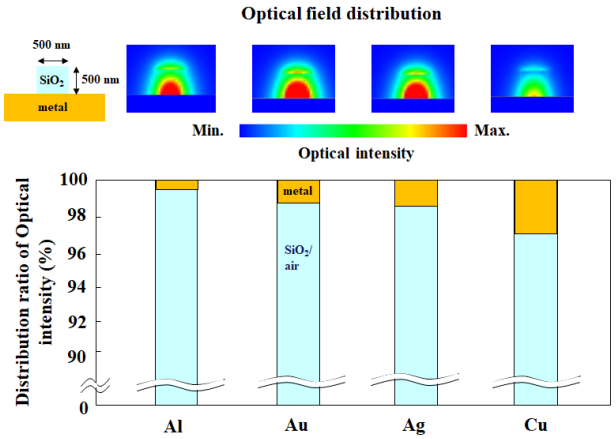

FIGURE 3. Calculated optical field distributions (upper images) and intensity distribution ratios of the optical field (lower plot) of SPPs on SiO_2-DLSP waveguides.

These results show that Au, Ag, and Al are appropriate metals for constructing plasmonic waveguides, and Al can be simultaneously used for merging plasmonic circuits with silicon ICs. Herein, however, Au was used in this study because of its chemical stability in the laboratory atmosphere.

III. SCALE OF LIGHTWAVE CIRCUITS

The scale of micro-optics employing optical fibers and planar lightwave circuits is larger than the wavelength of the signal lightwave. Waveguides comprising photonic crystals and high-refractive-index materials can be applied to sub-wavelength optics. For the range narrower than these scales in sub-wavelength optics, however, optical signals scarcely pass through the waveguides owing to the cutoff wavelength. For example, when a lightwave with a 1550 nm wavelength passes through a square cross-section silicon waveguide formed on a SiO_2 substrate, the cutoff wavelength was calculated to be a square between 200 nm (T) $\times$ 200 nm (W) and 300 nm (T) $\times$ 300 nm (W). The cross-sectional distribution of the optical power at the point $\sim$5 μm from the input ports is shown in Fig.4(a) for the Si waveguide sized 200 nm (T) $\times$ 200 nm (W). The transmitted optical field is primarily located at the interface between the silicon waveguide and the SiO_2 substrate, and very little is located in the Si waveguide because of the cut-off wavelength. This is because the refractive index of the substrate is higher than that of air, and therefore the optical power is mainly emitted to the SiO_2 substrate. This situation is similar to that of a SiN_x waveguide on a SiO_2 substrate, though the width and thickness of the waveguide at the cut-off waveguide is estimated as 600 nm (T) $\times$ 600 nm (W) because the refractive index of SiN_x is approximately half that of Si.

Conversely, the optical field of SPPs is bound to the collective oscillating electrons in the metal and pass through the plasmonic waveguide with the size 200 nm (T) $\times$ 200 nm (W), as shown in Fig.4(b). The width of the plasmonic waveguide can be reduced to the range of less than 100 nm. For plasmonic waveguides, however,

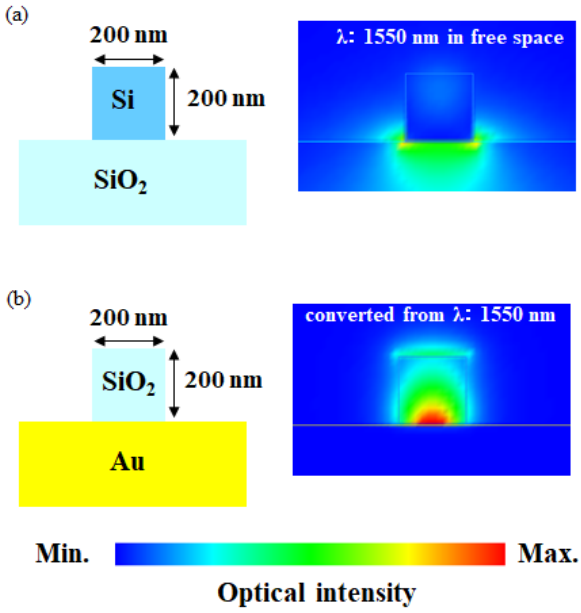

FIGURE 4. Cross-sectional view of the optical field distribution of (a) a lightwave in a Si waveguide and (b) SPPs in a plasmonic waveguide. The wavelength of propagating light is set at 1550 nm in free space, and the SPPs are converted from the light wave. The refractive indices of Si and SiO_2 are set at 3.51 and 1.45, respectively, in a wavelength band of 1550 nm.

another important factor emerges. Specifically, as the width of waveguide decreases, the confinement factor, which indicates the ratio of the optical field within the waveguide to the total, gradually decreases, and the majority of the optical field propagates in a region outside of the waveguide. This results in an increase in the propagation length (Fig.5). If a plasmonic waveguide is placed alone, we can fabricate a plasmonic waveguide with a relatively low loss in the nanophotonics range, but the leakage of the optical field becomes high. If multiple waveguides are set in circuits, the optical field leakage results in cross-talk because the leaked optical field is easily coupled to the neighboring waveguides. These propagation characteristics of SPPs strongly depend on the waveguide structures [22] and materials used. We can fabricate plasmonic waveguides in the nanophotonics range using suitable waveguide structures that take these characteristics into consideration.

IV. SIGNAL TRANSMISSION PROPERTIES

In optical fiber transmission systems, the quality (i.e., signal-to-noise ratio or bit error rate (BER)) were determined by several factors including quantum noise and chromatic and mode dispersion in the transmission waveguides. In the micro- and nanophotonic scale, signal transmission is a miniaturization of such optical fiber systems, and the issues observed in the optical fiber transmission systems also appear in these micro- and nanoscale transmission circuits. The characteristic issue among these is chromatic dispersion, although the transmission lengths are many orders of magnitude shorter than those of optical fiber systems. The chromatic dispersion is a more severe problem for silicon

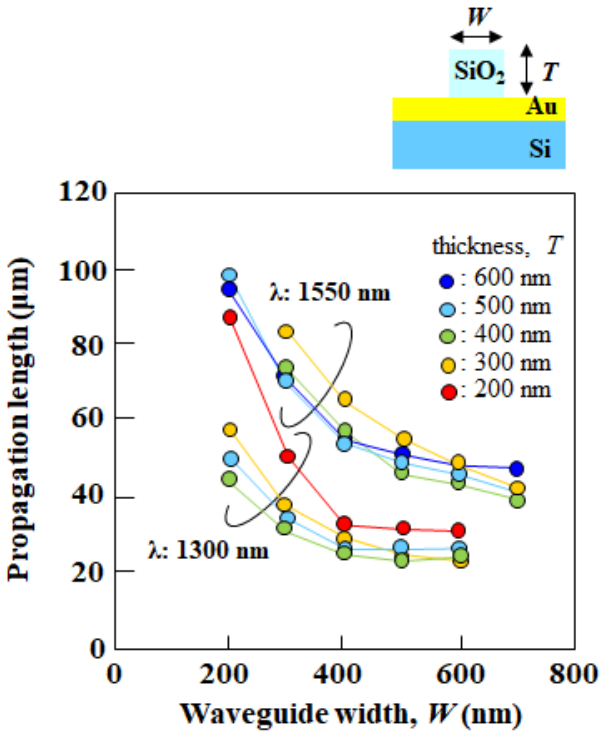

FIGURE 5. Propagation length for various thicknesses of plasmonic waveguides.

waveguides using a propagating lightwave. Although the dispersion varies depending upon the wavelength used and the configuration of the waveguides, the values in silicon waveguides are several orders of magnitude larger than those in silica fibers [23]–[25]. The chromatic dispersion in a plasmonic waveguide with a SiO_2 stripe sized 500 nm (T)× 500 nm (W) and fabricated on a Au film (see Fig. 5) was roughly calculated to be −1000 ps/(nm·km) in the near-infrared range and was slightly smaller than those of silicon waveguides. Though the influence of the dispersion varies with the waveguide configurations, it will be small in plasmonic waveguides because the transmission distance is much shorter than that in silicon photonics.

A new factor must be considered in plasmonic circuits, however. For signals with a wide wavelength spectra, the wavelength-spectral shapes of the plasmonic signals deform and decrease from the higher frequency side during propagation for a few hundred micrometers [19], [26]. This is owing to the frequency dependence of the collective oscillation of electrons. Therefore, a narrow spectral width is an important factor for data transmission for circuits extending a relatively long distance. The frequency (or wavelength) spectrum of SPPs converted from a coherent light beam can be expressed using the Lorentz function, such that

$$S_0(\omega) = w/[(\omega - \omega_0)^2 + w^2], \tag{3}$$

where w is the half width at half maximum of the spectrum and ω_0 is the center angular frequency of the spectrum. According to the Wiener-Khintchine theorem,

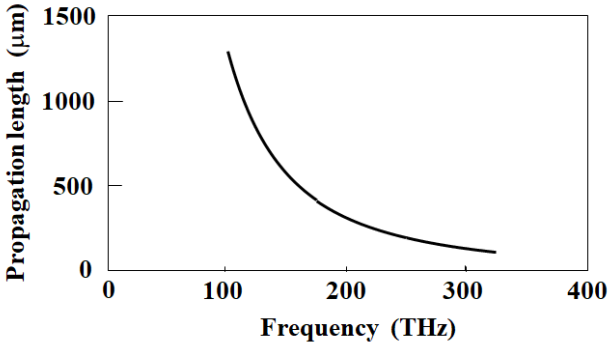

FIGURE 6. SPP propagation length on Au surface as a function of oscillation frequency based on the Drude model.

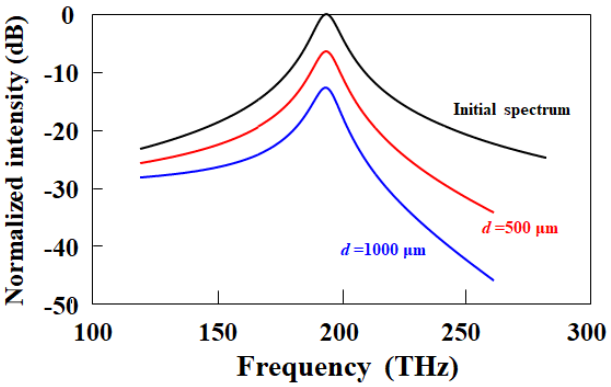

FIGURE 7. Change in spectral line shape as a function of frequency during propagation.

the spectrum of SPPs after a transmission distance, d, can be given by [27]

$$S(\omega, d) = S_0(\omega) \exp(-d/d_p), \tag{4}$$

where d_p is the propagation length (see Eq.(1)) that depends on the frequency. Based on the Drude model, the dielectric constant of the metal is expressed here as

$$\varepsilon_m(\omega) = \varepsilon_0\{1 - [\omega_p^2/(\omega^2 + i\omega/\tau)]\}, \tag{5}$$

where ε_0 is the dielectric constant of air, ω_p is the plasma frequency, and τ is the mean collision time in the metal. Using Eqs.(1), (2), (5), $\omega_p = 1.4 \times 10^{16}$ rad/s, and $\tau = 8.64 \times 10^{-15}$ s [28] for Au, the calculated propagation length on the Au surface as a function of SPP frequency is plotted in Fig.6. The calculated spectra after a transmission distance of 0, 500, and 1000 μm for a signal with $w = 5$ THz (∼40 nm) are compared in Fig.7. It can be seen that the shape of the spectrum gradually deformed on the high-frequency side of the spectrum as the transmission distance increased.

Based on these results, a narrow wavelength spectral width is required for plasmonic signals to stabilize signal shapes during transmission for relatively long distances. In addition, single-mode waveguides are favorable to suppress the instability caused by signal deformation through the

multimode dispersion, where the transmission speed varies slightly for each mode in the multimode waveguide.

In optical circuits, very short optical pulses with a width around 1 ps or less are often transmitted as a frequency comb pulse train or solitons [29], [30]. These pulses are generated from optical sources with wide wavelength spectra, a few nanometers or more in width, although the width depends on the pulse generation techniques. Here, the chromatic dispersion is suppressed using the nonlinear optical effect of the waveguides. Optical pulse transmission techniques using the optical nonlinear effect will be also applicable to plasmonic circuits. When the wavelength spectral width is a few nanometers, the pulse shape deformation induced by the collective oscillation of electrons and the chromatic dispersion will be negligible if the transmission distance is less than a few hundred micrometers.

In plasmonic waveguides, the number of photons (i.e., optical field) bound to the electrons gradually decreases owing to the ohmic loss caused by the collective oscillation of electrons in the metal and the scattering loss of the optical field. Thus, the number of signal-carrying photons decreases and its power level approaches the level of noise, caused primarily by quantum (i.e., shot or white) noise. The propagation length is therefore limited by quantum noise. Under this condition (quantum noise limit), the energy loss per single transmitted bit and the signal delay for a plasmonic waveguide (Ag rods) were calculated and compared with those of electric signals in Si ICs [31]. Here, the electric transmission energy in the ICs is expressed as $(1/2)CLV^2$ (C: capacitance per unit transmission length, L: transmission length, V: transistor operation voltage). Following [31], we have discussed the plasmonic loss and signal time delay for SiO_2 stripe DLSP waveguides [19], where the signal time delay was approximately two orders of magnitude smaller than that of electric signals. Furthermore, in transmission systems employing intensity modulation direct detection or frequency-shift keying coherent detection techniques, the energy loss per single transmitted bit of a plasmonic signal was lower than that of an electric signal even under a BER of 10^{-30} when the plasmonic circuits were formed within a range of less than a few hundred square micrometers. The scale of a few hundred square micrometers is sufficient for forming plasmonic circuits.

In addition to the plasmonic intensity signal transmission, coherent signal transmissions could be performed when high-coherence (i.e., narrow spectral linewidth) optical sources were used. We previously reported on the feasibility of coherent signal transmission through a plasmonic waveguide integrated metal-oxide-semiconductor field-effect transistors (MOSFETs) using a self-delayed homodyne technique [32], [33]. In those studies, we observed beat signals with a peak at 0 Hz outputted from a MOSFET. These beat signals were also observed using the self-delayed heterodyne technique.

A schematic diagram of the self-delayed heterodyne detection system is shown in Fig.8(a). In this system, a light

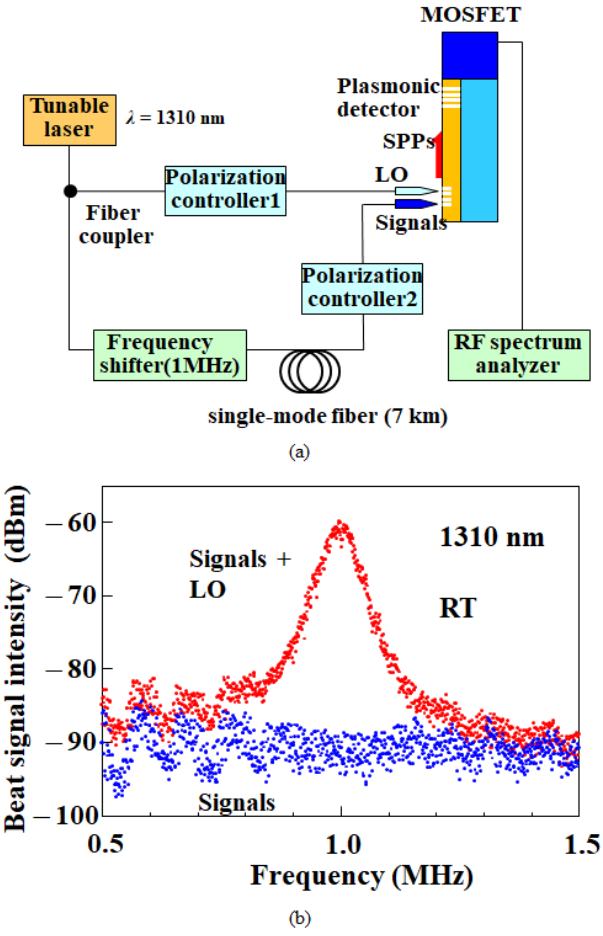

FIGURE 8. (a) Self-delayed heterodyne system setup and (b) beat signal outputted from the MOSFET.

beam emitted from an optical source with narrow spectral linewidth (i.e., less than a few tens of kilohertz) was divided into two optical paths. One light beam (termed "LO": local oscillator) was placed directly incident on the grating built on a plasmonic waveguide connected to the gate of a MOSFET. The frequency of the other light beam (termed "Signals") was increased by 1 MHz with a frequency shifter and then made incident on the grating after transmission through 7 km of optical fiber. The polarization of each light beam was controlled to be perpendicular to the slits, where the incident light beams were converted to plasmonic signals. When the two light beams (Signals + LO in Fig.8(a)) were incident to the slits, the beat signal clearly registered at 1 MHz in the electrical output of the MOSFET (Fig.8(b)), while no beat signal appeared when only one beam was incident (Signals in Fig.8(b)).

These results show that coherent signal detection using heterodyne as well as homodyne techniques are applicable to an integrated circuit comprising a plasmonic waveguide and MOSFET. Consequently, we can transmit coherent optical signals through plasmonic circuits and fabricate their integration with electronic circuits with no issues. In plasmonic circuits, the transmission of multiple signals for coherent

and intensity signals using WDM and frequency-division multiplexing (FDM) techniques can be performed within micro/nano-circuits in a manner similar to that of commercial optical fiber transmission systems.

V. PERFORMANCE OF PLASMONIC CIRCUITS

This section contains a detailed discussion regarding the transmission speed and loss of plasmonic circuits, which are compared with lightwave circuits such as silicon waveguides.

A. TRANSMISSION SPEED

The transmission speed of electric signals is determined by the capacitance and resistance of the circuit, while that of plasmonic signals is determined by the group velocity governed by the dispersion relation in the waveguide. In silicon waveguides, the transmission speed of optical signals is also determined by the group velocity in a manner similar to the case of SPPs. The transmission speed is, therefore, essentially the same, although the scale of lightwave circuits in silicon photonics is larger than that of plasmonic circuits. The refractive index of the Si waveguide is between 4 and 5 in the 1310 and 1550 nm bands, [23]–[25] and is greater than that of plasmonic DLSP waveguides such as a SiO_2 stripe on a metal film. Therefore, the propagation velocities of lightwave signals in silicon waveguides are lower than those of plasmonic signals. However, the circuit operation speeds related to the propagation signal velocities will be governed by the operation speed of the optoelectronic components, such as the photo- or plasmonic-detectors in silicon photonics and plasmonics.

B. TRANSMISSION LOSS

In electronic circuits such as the wiring in silicon ICs, as the wiring width decreases, the transmission loss increases owing to the increase in electric resistance and stray capacitance. In silicon waveguides using propagating light waves in the 1310 and 1550 nm bands, the losses primarily induced by light scattering via side-wall roughness in the waveguide were a few tens of decibels per centimeter or less in the waveguides with sub-wavelength widths [23], [34]–[38]. In addition, the losses were over two orders of magnitude smaller than those of plasmonic waveguides in a similar sub-wavelength range. In the nanophotonics range, however, the propagation loss quickly increased as the waveguide width decreased from the viewpoint of signal transmission characteristics, as discussed in Sec. III. From the physical phenomena, the propagation loss quickly increased as the waveguide width approached the waveguide cut-off wavelength. Near the cut-off wavelength, the amount of light emitted from the waveguide significantly increased in addition to the scattering loss, as shown in Fig.4(a). For waveguide widths less than a few hundred nanometers, therefore, only plasmonic waveguides can be currently applied to optical circuits.

In plasmonic circuits, transmission loss varies widely with the waveguide structure. A metal stripe and a SiO_2/metal stripe waveguide on Si exhibited an increase in transmission

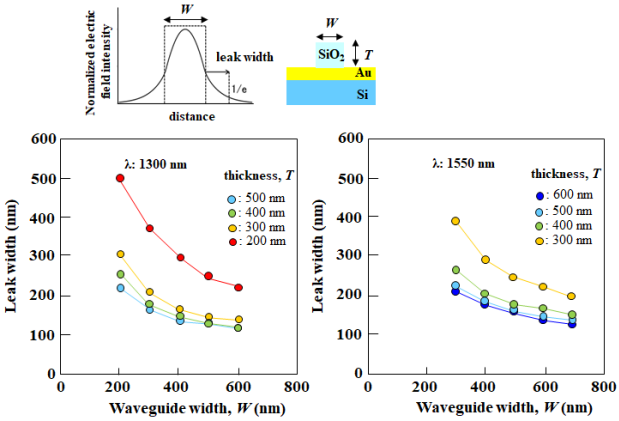

FIGURE 9. Leak width of the optical field for a plasmonic waveguide.

loss as the waveguide width decreased, while the transmission loss of a SiO_2 stripe on a metal film rapidly decreased as the width decreased [22]. The ohmic loss of SPPs in the waveguide shown in Fig.5 quickly decreased as the waveguide width narrowed, because the area within which the optical field contacted the metal was reduced. However, as shown in Fig.9, the distribution of the SPP optical field spread out from the waveguide as the waveguide width decreased. The leak width of the optical field from the side-wall of the waveguide limits the degree of integration and governs the circuit configurations.

C. DEGREE OF INTEGRATION AND METAL/INSULATOR/METAL WAVEGUIDE

In silicon ICs, the degree of integration is indicated by the half pitch between metal wires. In plasmonic circuits, the half pitch is determined by the leak width of the SPP optical field, as discussed in Sec. III regarding the suppression of cross-talk between waveguides. If we consider only the scale of the waveguides, plasmonic grooved and hybrid waveguides [6]–[14] are favorable. By employing these waveguide structures, we can fabricate nanoscale waveguides less than 100 nm without optical field leak issues. However, as described in Sec. I, simple waveguides are favorable for construction of plasmonic components such as multiplexers and demultiplexers in high-density integrated circuits. The SiO_2 stripe DLSP waveguides easily form functional networks such as on-chip interconnects employing WDM techniques and logic circuits [19], [39], [40], although the circuit scales are somewhat large. These scale and functionality issues can be solved by employing MIM structures with the DLSP waveguides. The MIM structure is formed by adding a metal layer on the dielectric film. Some plasmonic components based on the MIM structure have previously been experimentally or numerically demonstrated [11]–[16]. Here, a single-mode waveguide and a multiplexer for 1310 and 1550 nm band WDM circuits are experimentally examined and the feasibility of nanoscale functional plasmonic circuits is discussed.

The authors have indicated that a plasmonic multiplexer for 1300 and 1550 nm wavelength bands was fabricated within

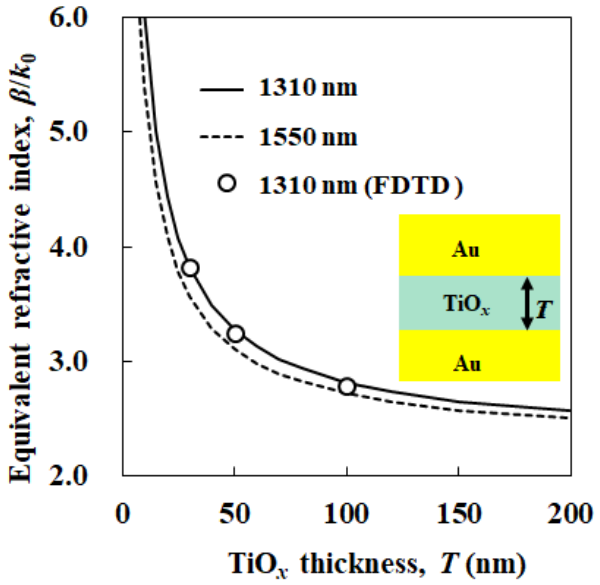

FIGURE 10. Equivalent refractive index of Au/TiO_x/Au structure as a function of TiO_x layer thickness in 1310 and 1550 nm bands. β and k_0 are the propagation constant (= $n_{eq}k_0$) and wavenumber in free space, respectively. The open circles indicate the numerical results obtained by the FDTD method.

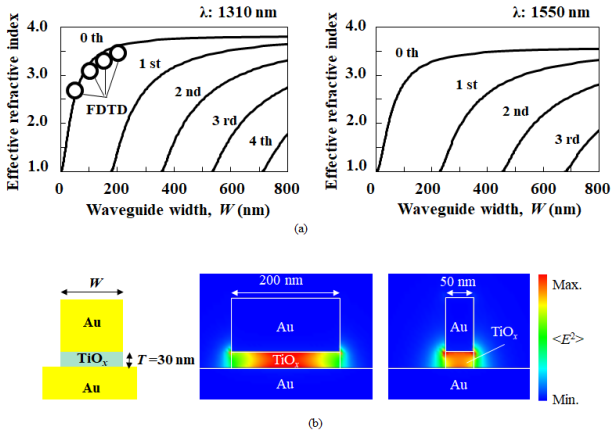

FIGURE 11. (a) Effective refractive index of Au/TiO_x mesa structure as a function of the mesa width in 1310 nm (left plot) and 1550 nm (right plot) bands. The inserted number rankings indicate the mode numbers. (b) Cross-sectional view of the plasmonic power distribution of the mesa structure with 50 nm (right image) and 200 nm (center image) width.

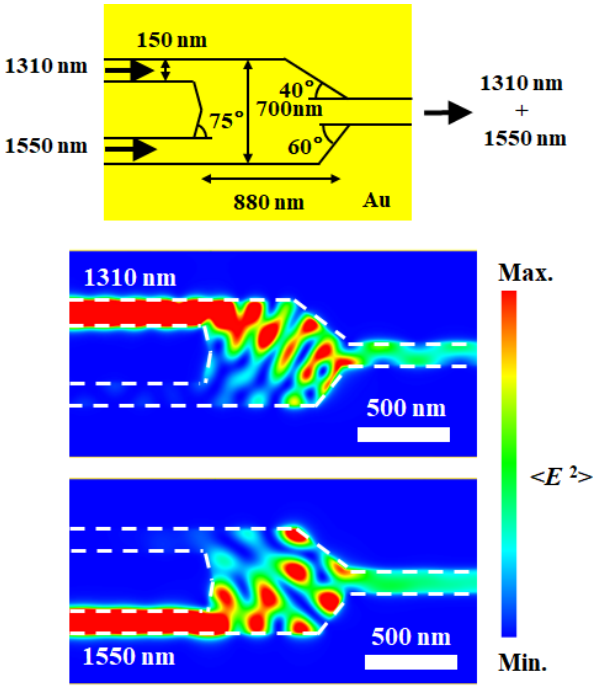

FIGURE 12. Design of the 1310 and 1550 nm wavelength multiplexer with a tapered structure (top image) and the numerically calculated SPP intensity distribution within the TiO_x layer for the 1310 nm (center image) and 1550 nm (bottom image) band using the 3D-FDTD method.

a length of less than 1 μm using a Au (100 nm)/sputtered TiO_x film (30 nm)/Au-layer structure [19]. The details of the MIM multiplexer are discussed here to examine the feasibility of plasmonic components in a range of less than 1 μm. The designs for the waveguide and multiplexer were carried out by the following two-step procedure: (1) The equivalent refractive indices of Au/TiO_x/Au were calculated by solving the so-called characteristic equation of the waveguide. The equivalent refractive index is shown in Fig.10 as a function of the thickness of TiO_x layer for the 1310 and 1550 nm wavelength bands. Here, the refractive indices of Au were set at $0.41 + 8.37i$ in the 1310 nm band and $0.56 + 11.5i$ in the 1550 nm band [21]. The refractive index quickly increases as the thickness of the TiO_x layer decreases. (Here, the refractive index of the thick TiO_x was experimentally determined to be 2.261 in the 1310 nm band and 2.255 in the 1550 nm band by ellipsometry.) (2) Using the equivalent refractive index, the effective refractive index was calculated as a function of the width of the mesa-type waveguide (Fig.11). We can see that plasmonic signals with the zeroth mode can propagate even in a waveguide with width less than 100 nm. The cross-sectional views of the SPP power distribution are given in Fig.11(b).

Based on these results, the width of the single-mode waveguides (input and output waveguides) was set at 150 nm, and the size of the multimode interferometer (MMI, (multimode waveguide)) was set at 700 nm (width) × 900 nm (length). This waveguide width allows the zeroth- to third-order modes in the 1300 nm wavelength band and the zeroth- to second-order modes in the 1550 nm wavelength band into the MMI (see Fig.11(a)), and the length was set at the length generating the mirror image of all modes [41]. In addition, to reduce the reflection of SPPs within the MMI, tapered structures were introduced as shown in Fig.12. The introduction of these structures reduced the reflection in the MMI by 3 dB in the 1310 nm band and 5 dB in the 1550 nm band. Fig.13 shows the scanning electron microscope (SEM) images of the fabricated waveguides for the 1310 and 1550 nm bands. Fig.14 shows the intensity distributions obtained numerically by the 3D-FDTD method and experimentally by scanning near-optical field microscopy (SNOM) on the upper Au layer. The theoretical

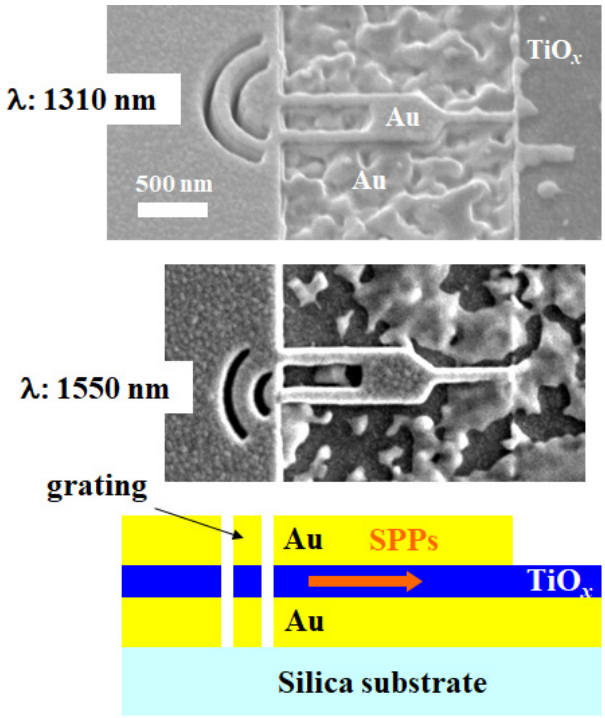

FIGURE 13. SEM images of fabricated 1310- and 1550-nm wavelength multiplexers.

and experimental distributions agree well with each other, and the multiplexing operation is confirmed. The loss in the multiplexer increased in the MIM structure because the size reduction induced an increase in the refractive index, and the wavelength was shortened by the change. The insertion loss calculated using the 3D-FDTD method was estimated as 7.5 dB in the 1310 nm band and 6.0 dB in the 1550 nm band. The insertion loss is primarily caused by ohmic loss generated on the upper and lower metal films.

The propagation loss of a single-mode waveguide is shown in Fig.15 in the 1310 nm wavelength band. As the width decreases, the propagation loss gradually decreases. However, the optical field leak from the side-walls is negligible small in the simulations and experimentally estimated as less than 100 nm, as shown in Figs.11(b) and 14. The value of the half pitch, which is a measure of the degree of integration, can be set at less than 100 nm for functional plasmonic components as well as waveguides (i.e., signal transmission lines).

VI. FEASIBILITY OF PLASMONIC CIRCUIT

In the previous sections, the plasmonic circuits were numerically and experimentally discussed in the transmission range of less than a few hundred micrometers and compared with silicon waveguide circuits. The plasmonic circuits operated well even for waveguides with nano-scale cross-sections, while lightwave signal transmission was difficult owing to the transmission loss increase induced by the cut-off wavelength in the waveguides. The transmission loss results, however, reversed in the waveguide with a cross-sectional area more than a few hundred square nanometers. When compared

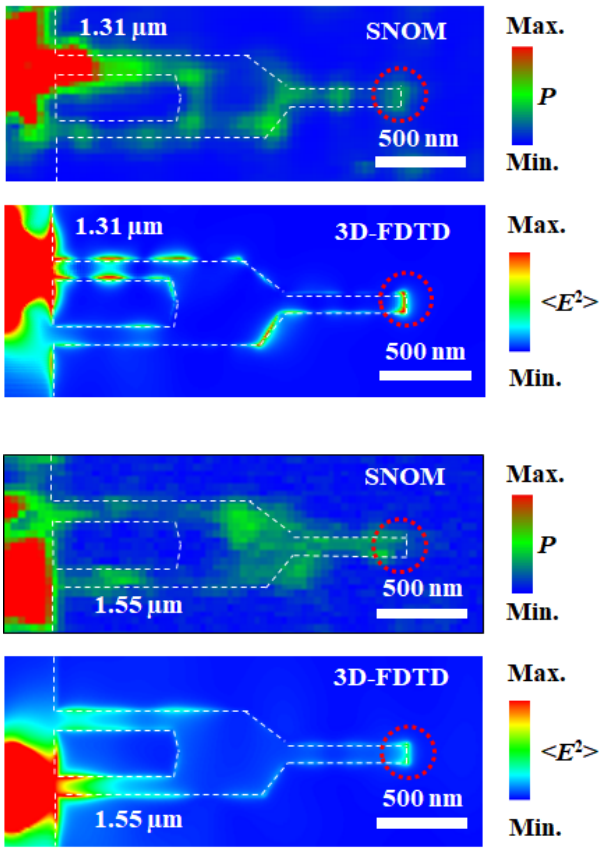

FIGURE 14. Intensity distribution of SPPs obtained by the 3D-FDTD method and SNOM.

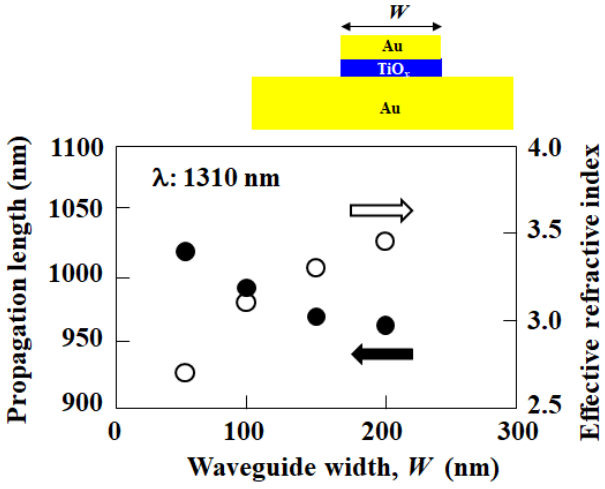

FIGURE 15. Propagation length and effective refractive index of the Au/TiO_x mesa structure on a Au layer as a function of the mesa width.

with the electric circuits, the plasmonic signal transmissions within a few hundred micrometers were effective because of the lower transmission loss [19]. Therefore, the plasmonic circuits will be valid in small-scale areas such as on-chip interconnections between processors and memories. Additionally, the connection part between lightwave and

electronic circuits will be adaptive area for size matching. The circuits can be extended to functional networks such as logic circuits [39], [40] within the permissible range of the circuit loss.

A. CONFIGURATION OF PLASMONIC CIRCUIT

In plasmonic circuits, signal deformation owing to the dispersion and frequency dependence of the collective electron oscillation (see Figs. 6 and 7) must be avoided to maintain the transmission quality (i.e., signal-to-noise ratio and BER). Additionally, coherent plasmonic signals are favorable for operation of the multimode waveguides as MMIs (i.e., phase controllers, multiplexers, and demultiplexers). Consequently, at present, a coherent off-chip laser with a single-longitudinal mode was applied to the circuits. From the outside of the chip, a coherent light beam was incident to the gratings built in the waveguide and converted to high-coherence plasmonic signals. The conversion efficiency of this configuration was numerically and experimentally discussed and estimated to be a few tens of percent [19]. The light beam can also be incident to the grating through a silicon waveguide.

A plasmonic detector-integrated MOSFET can be used to connect the output ports to electronic circuits, where plasmonic signals are converted to electric signals. Previously, a plasmonic detector-integrated MOSFET composed of two Si MOSFETs (for signal amplification and impedance matching) and slits built in the gate electrode of a MOSFET was used in this way [42]. The efficiency of a prototype of the receiver unit was estimated to be more than 0.30 mA/mW, even in the 1550-nm-wavelength band [19]. The structure of the plasmonic receiver unit was quite simple, and plasmonic waveguides were directly connected to the MOSFET gate via the slits.

Regarding other components such as amplifiers and modulators, an amplifier will be unnecessary for on-chip interconnection between the processor and memory area. On-chip modulators have been successfully developed and those will be applied for plasmonic circuits [43], [44].

B. CIRCUIT FLEXIBILITY

Plasmonic circuits are normally planar circuits, and crossing and bending waveguides are useful to increase the flexibility. The feasibility of a crossing plasmonic waveguide has been shown in [45]. At various crossing angles of single-mode waveguides, the insertion loss of the crossing waveguide was experimentally estimated to be approximately 1.5 dB, and the cross-talk of transmitted signals was experimentally obtained to be less than −7 dB in the 1300 nm wavelength band.

In the DLSP waveguides, optical confinement in the surface (lateral) direction is primarily realized with a dielectric mesa structure, and thus the performance is essentially similar to the case of a silicon waveguide. The bending losses of DLSP waveguides have been numerically and experimentally reported in various works [5], [17], [46]. The loss of a bending waveguide is caused by ohmic and radiation losses at the bend area, where radiation loss is dominant in

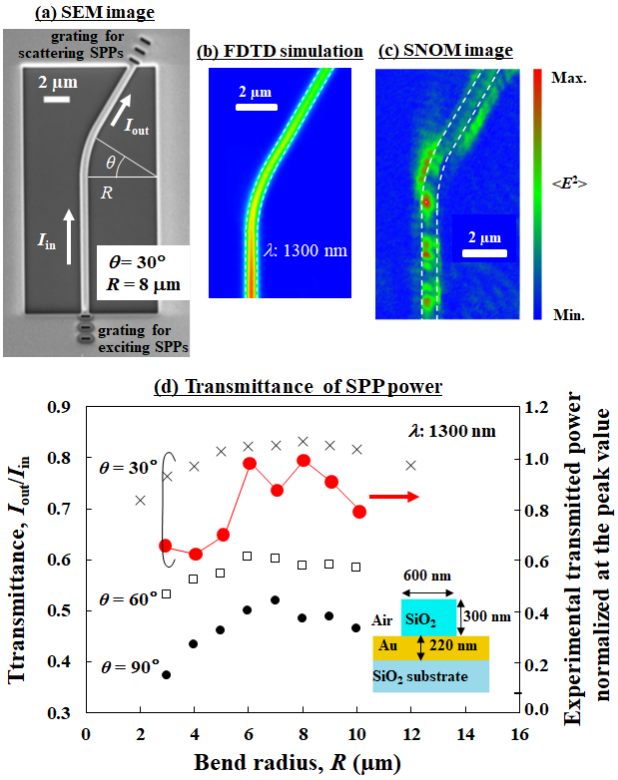

FIGURE 16. Signal transmission in a bending SiO_2-DLSP waveguide. (a) SEM image of fabricated bending waveguide, (b) simulation results using FDTD method, (c) SNOM image, (d) plasmonic power transmittance determined with ohmic and radiation loss. Inset in (d) is the waveguide cross-section schematic.

waveguides with small bending radii and the ohmic loss gradually increases as the radius increases [46]. The radiation loss depends on the waveguide shape, bend angle, bend radius, and signal wavelength. In the 1550 nm wavelength band, a total transmission loss of less than 2 dB was calculated even for 90°-bend waveguides [5], [17]. In the 1300 nm wavelength band, the transmittance of plasmonic signals in bending SiO_2-DLSP waveguides is shown in Fig.16. Fig.16(b) and 16(c) shows the intensity distribution of SPPs in the bending single-mode waveguide, obtained using the FDTD method and SNOM. Although the radiation loss is large in the area of the small bend radius, we can use plasmonic bending waveguides under low loss by selecting a suitable bend angle and radius.

In 1300 and 1550 nm wavelength bands, the radiation loss of a bending waveguide is not inferior to those in high-refractive-index waveguides such as silicon waveguides [47], although the total loss tends to be larger because of ohmic loss. Using these crossing and bending waveguides, flexible plasmonic circuits can be constructed.

C. SIGNAL MULTIPLEXING

As mentioned in Sec. IV, the signal transmission in plasmonic and other photonic circuits is a miniaturization of optical fiber systems. Thus, signal multiplexing techniques such as FDM and WDM are available in these circuits, and plasmonic circuits are especially suited to introduce such techniques to

nanophotonics-scale circuits. Using the coherent detection techniques discussed in Sec. IV, FDM signals can be transmitted in the circuits, although another waveguide is required to induce beating of the transmitting SPPs (i.e., local oscillator) with the transmitted signals. In this technique, the transmitted signal intensity is amplified with the local oscillator via the beating. Using the optical heterodyne detection technique, the transmitted plasmonic signals have been amplified by approximately 14 dB by mixing the transmitted signals and the local oscillator [32].

For WDM techniques, the so-called dense WDM with a channel spacing of 100 GHz and coarse WDM with a channel spacing of 20 nm, which are commercially used in optical fiber communication systems, cannot be applied to plasmonic circuits because of the circuit scale. Multiplexing and demultiplexing signals with different wavelengths cannot be spatially carried out within the range of a few hundred micrometers. In such a nano/micro-scale circuit, however, a very sparse WDM circuit including two signals in a 1300 and a 1550 nm wavelength can be formed, as discussed in Sec. V and reported in Ref. [48], [49]. In the plasmonic WDM circuits, the input ports are easily fabricated using a grating. However, the output ports must be electrically separated to connect to the MOSFET gate electrodes in the WDM circuits because the metal layer is common in each waveguide. Introducing an electrical separation gap to the plasmonic waveguides [50], each plasmonic signal can be connected to each MOSFET gate. The feasibility of such configuration has been discussed in Ref. [19].

VII. SUMMARY

The characteristics of plasmonic circuits at the scale of the nanophotonic range were discussed relative to electronic and propagating lightwave circuits. The scale of plasmonic components could be reduced to less than 1 μm. This enabled on-chip interconnects or functional circuits employing multi-access techniques such as WDM techniques to be constructed within a scale of less than a few tens of micrometers. In this range, the transmission loss of plasmonic signals in the 1310 and 1550 nm wavelength bands was lower than that of electric signals. Although the transmission loss of a lightwave propagating in silicon waveguides was much lower than that of plasmonic signals, plasmonic circuits were superior to the high-refractive-index waveguides such as silicon waveguides with cross-sections less than a few hundred square nanometers, from the viewpoint of transmission loss.

In the nanophotonic range, the degree of integration for plasmonic circuits is not governed by the transmission loss but by the width of the plasmonic signal optical field leak from the side-walls of the waveguides and components. Employing metal/insulator/metal structures in plasmonic circuits is a valid way to heighten the integration density, and the effectiveness is numerically and experimentally confirmed, despite the increase in the transmission loss.

It was numerically confirmed that the optical source of the plasmonic signals should have a narrow spectral width. This effectively suppressed the signal shape deformation caused by the frequency (wavelength) dependence of the collective oscillation of electrons in the plasmonic signals, in addition to the chromatic dispersion. The transmission losses of waveguides comprising Al, Au, and Ag were approximately equivalent, and much lower than that comprising Cu. These differences were caused by the variation in plasmonic signal penetration depth into the metal (i.e., difference in ohmic loss).

From these discussions, it can be said that plasmonic circuits including waveguides and components are promising optical techniques in the nanophotonic range.

ACKNOWLEDGMENT

The authors would like to thank Dr. Moise Sotto, Assistant Professor, Toyohashi University of Technology, for his discussions on the behavior of high-refractive-index waveguides; and Ms. Asahi Sumimura, Stanley Electric Company Ltd., Dr. Masashi Fukuhara, Tsukuba Research Center, Hamamatsu Photonics K. K., and Mr. Hiroki Sakai, MuRata Manufacturing Company Ltd. for their support and discussions on the design and fabrication of plasmonic waveguides when they were enrolled at Toyohashi University of Technology.

REFERENCES

[1] J. Takahara and F. Kusunoki, "Guiding and nanofocusing of two-dimensional optical beam for nanooptical integrated circuits," *IEICE Trans. Electron.*, vol. 90, no. 1, pp. 87–94, Jan. 2007.

[2] F. Kusunoki, T. Yotsuya, J. Takahara, and T. Kobayashi, "Propagation properties of guided waves in index-guided two-dimensional optical waveguides," *Appl. Phys. Lett.*, vol. 86, no. 21, May 2005, Art. no. 211101.

[3] C. Reinhardt, S. Passinger, B. N. Chichkov, C. Marquart, I. P. Radko, and S. I. Bozhevolnyi, "Laser-fabricated dielectric optical components for surface plasmon polaritons," *Opt. Lett.*, vol. 31, no. 9, pp. 1307–1309, 2006.

[4] B. Steinberger, A. Hohenau, H. Ditlbacher, A. L. Stepanov, A. Drezet, F. R. Aussenegg, A. Leitner, and J. R. Krenn, "Dielectric stripes on gold as surface plasmon waveguides," *Appl. Phys. Lett.*, vol. 88, no. 9, Feb. 2006, Art. no. 094104.

[5] A. V. Krasavin and A. V. Zayats, "Passive photonic elements based on dielectric-loaded surface plasmon polariton waveguides," *Appl. Phys. Lett.*, vol. 90, no. 21, May 2007, Art. no. 211101.

[6] D. K. Gramotnev and S. I. Bozhevolnyi, "Plasmonics beyond the diffraction limit," *Nature Photon.*, vol. 4, no. 2, pp. 83–91, Feb. 2010.

[7] S. I. Bozhevolnyi, V. S. Volkov, E. Devaux, J.-Y. Laluet, and T. W. Ebbesen, "Channel plasmon subwavelength waveguide components including interferometers and ring resonators," *Nature*, vol. 440, no. 7083, pp. 508–511, Mar. 2006.

[8] R. F. Oulton, V. J. Sorger, D. A. Genov, D. F. P. Pile, and X. Zhang, "A hybrid plasmonic waveguide for subwavelength confinement and long-range propagation," *Nature Photon.*, vol. 2, no. 8, pp. 496–500, 2008.

[9] Y. Bian, Z. Zheng, X. Zhao, L. Liu, Y. Su, J. Liu, J. Zhu, and T. Zhou, "Nanoscale light guiding in a silicon-based hybrid plasmonic waveguide that incorporates an inverse metal ridge," *Phys. Status Solidi A*, vol. 210, no. 7, pp. 1424–1428, Jul. 2013.

[10] V. J. Sorger, Z. Ye, R. F. Oulton, Y. Wang, G. Bartal, X. Yin, and X. Zhang, "Experimental demonstration of low-loss optical waveguiding at deep subwavelength scales," *Nature Commun.*, vol. 2, no. 1, p. 331, Sep. 2011.

[11] E. N. Economou, "Surface plasmons in thin films," *Phys. Rev.*, vol. 182, no. 2, pp. 539–554, Jun. 1969.

[12] J. A. Dionne, L. A. Sweatlock, H. A. Atwater, and A. Polman, "Plasmon slot waveguides: Towards chip-scale propagation with subwavelength-scale localization," *Phys. Rev. B, Condens. Matter*, vol. 73, no. 3, Jan. 2006, Art. no. 035407.

[13] C.-I. Lin and T. K. Gaylord, "Multimode metal-insulator-metal waveguides: Analysis and experimental characterization," *Phys. Rev. B, Condens. Matter*, vol. 85, no. 8, Feb. 2012, Art. no. 085405.

[14] M. Ota and M. Fukuda, "Highly efficient on-chip excitation of orthogonal-polarized gap plasmons for a dense polarization multiplexing circuit," *Opt. Express*, vol. 26, no. 17, pp. 21778–21783, 2018.

[15] E. Verhagen, J. A. Dionne, L. Kuipers, H. A. Atwater, and A. Polman, "Near-field visualization of strongly confined surface plasmon polaritons in metal–insulator–metal waveguides," *Nano Lett.*, vol. 8, no. 9, pp. 2925–2929, Sep. 2008.

[16] Z. Han and S. He, "Multimode interference effect in plasmonic subwavelength waveguides and an ultra-compact power splitter," *Opt. Commun.*, vol. 278, no. 1, pp. 199–203, Oct. 2007.

[17] A. V. Krasavin and A. V. Zayats, "Active nanophotonic circuitry based on dielectric-loaded plasmonic waveguides," *Adv. Opt. Mater.*, vol. 3, no. 12, pp. 1662–1690, Dec. 2015, doi: 10.1002/adom.201500329.

[18] A. V. Krasavin and A. V. Zayats, "Benchmarking system-level performance of passive and active plasmonic components: Integrated circuit approach," *Proc. IEEE*, vol. 104, no. 12, pp. 2338–2348, Dec. 2016.

[19] M. Fukuda, Y. Tonooka, T. Inoue, and M. Ota, "Feasibility of plasmonic circuits for on-chip interconnects," *Solid-State Electron.*, vol. 156, pp. 33–40, Jun. 2019.

[20] J. B. Khurgin, "How to deal with the loss in plasmonics and metamaterials," *Nature Nanotechnol.*, vol. 10, no. 1, pp. 2–6, Jan. 2015.

[21] E. D. Palik, *Handbook of Optical Constants of Solids*. New York, NY, USA: Academic, 1985.

[22] S. Okahisa, K. Nakayama, Y. Nakayama, Y. Ishii, and M. Fukuda, "Guiding properties of 1.31-and 1.55-μm-wavelength surface plasmon polaritons on striped waveguides on silicon and their wavelength-selective detection," *J. Lightw. Technol.*, vol. 35, no. 13, pp. 2702–2711, Jul. 1, 2017.

[23] T. Horikawa, D. Shimura, H. Okayama, S.-H. Jeong, H. Takahashi, J. Ushida, Y. Sobu, A. Shiina, M. Tokushima, K. Kinoshita, and T. Mogami, "A 300-mm silicon photonics platform for large-scale device integration," *IEEE J. Sel. Topics Quantum Electron.*, vol. 24, no. 4, pp. 1–15, Jul. 2018.

[24] E. Dulkeith, F. Xia, L. Schares, W. M. J. Green, and Y. A. Vlasov, "Group index and group velocity dispersion in silicon-on-insulator photonic wires," *Opt. Express*, vol. 14, no. 9, pp. 3853–3863, May 2006.

[25] A. C. Turner, C. Manolatou, B. S. Schmidt, M. A. Foster, J. E. Sharping, A. L. Gaeta, and M. Lipson, "Tailored anomalous group-velocity dispersion in silicon channel waveguides," *Opt. Express*, vol. 14, no. 10, pp. 4357–4362, May 2006.

[26] T. Aihara, "Study of surface plasmon interconnections on silicon chips," Ph.D. dissertation, Dept. Elect. Electron. Inf. Eng., Toyohashi Univ. Technol., Toyohashi, Japan, 2014. no. 712, ch. 3.

[27] T. Aihara and M. Fukuda, "Transmission properties of surface-plasmon-polariton coherence," *Appl. Phys. Lett.*, vol. 100, no. 21, May 2012, Art. no. 213115.

[28] W. L. Barns, "Surface plasmon–polariton length scales: A route to sub-wavelength optics," *J. Opt. A, Pure Appl. opt.*, vol. 8, no. 4, pp. S87–S93, 2006.

[29] G. A. Sefler and K.-I. Kitayama, "Frequency comb generation by four-wave mixing and the role of fiber dispersion," *J. Lightw. Technol.*, vol. 16, no. 9, pp. 1596–1605, 1998.

[30] R. Wu, V. Torres-Company, D. E. Leaird, and A. M. Weiner, "Supercontinuum-based 10-GHz flat-topped optical frequency comb generation," *Opt. Express*, vol. 21, no. 5, pp. 6045–6052, 2013.

[31] J. A. Conway, S. Sahni, and T. Szkopek, "Plasmonic interconnects versus conventional interconnects: A comparison of latency, crosstalk and energy costs," *Opt. Express*, vol. 15, no. 8, pp. 4474–4484, 2007.

[32] T. Aihara, H. Sakai, A. Takeda, S. Okahisa, M. Fukuhara, M. Ota, Y. Ishii, and M. Fukuda, "Coherent plasmonic interconnection in silicon-based electrical circuit," *J. Lightw. Technol.*, vol. 33, no. 10, pp. 2139–2145, May 15, 2015.

[33] H. Sakai, S. Okahisa, Y. Nakayama, K. Nakayama, M. Fukuhara, Y. Kimura, Y. Ishii, and M. Fukuda, "Plasmonic and electronic device-based integrated circuits and their characteristics," *Solid-State Electron.*, vol. 125, pp. 240–246, Nov. 2016.

[34] P. Dumon, W. Bogaerts, V. Wiaux, J. Wouters, S. Beckx, J. Van Campenhout, D. Taillaert, B. Luyssaert, P. Bienstman, D. Van Thourhout, and R. Baets, "Low-loss SOI photonic wires and ring resonators fabricated with deep UV lithography," *IEEE Photon. Technol. Lett.*, vol. 16, no. 5, pp. 1328–1330, May 2004.

[35] Y. A. Vlasov and S. J. McNab, "Losses in single-mode silicon-on-insulator strip waveguides and bends," *Opt. Express*, vol. 12, no. 8, pp. 1622–1631, Apr. 2004.

[36] T. Tsuchizawa, K. Yamada, H. Fukuda, T. Watanabe, J.-I. Takahashi, M. Takahashi, T. Shoji, E. Tamechika, S. Itabashi, and H. Morita, "Microphotonics devices based on silicon microfabrication technology," *IEEE J. Sel. Topics Quantum Electron.*, vol. 11, no. 1, pp. 232–240, Jan. 2005.

[37] R. Takei, S. Manako, E. Omoda, Y. Sakakibara, M. Mori, and T. Kame, "Sub-1 dB/cm submicrometer-scale amorphous silicon waveguide for backend on-chip optical interconnect," *Opt. Express*, vol. 22, no. 4, pp. 4779–4788, Feb. 2014.

[38] C. Bellegarde, E. Pargon, C. Sciancalepore, C. Petit-Etienne, V. Hugues, D. Robin-Brosse, J.-M. Hartmann, and P. Lyan, "Improvement of sidewall roughness of submicron SOI waveguides by hydrogen plasma and annealing," *IEEE Photon. Technol. Lett.*, vol. 30, no. 7, pp. 591–594, Apr. 1, 2018.

[39] M. Ota, A. Sumimura, M. Fukuhara, Y. Ishii, and M. Fukuda, "Plasmonic-multimode-interference-based logic circuit with simple phase adjustment," *Sci. Rep.*, vol. 6, no. 1, p. 24546, Jul. 2016.

[40] M. Fukuda, R. Watanabe, Y. Tonooka, and M. Ota, "Feasibility of cascadable plasmonic full adder," *IEEE Photon. J.*, vol. 11, no. 4, pp. 1–12, Aug. 2019.

[41] L. B. Soldano and E. C. M. Pennings, "Optical multi-mode interference devices based on self-imaging: Principles and applications," *J. Lightw. Technol.*, vol. 13, no. 4, pp. 615–627, Apr. 1995.

[42] T. Aihara, M. Fukuhara, A. Takeda, B. Lim, M. Futagawa, Y. Ishii, K. Sawada, and M. Fukuda, "Monolithic integration of surface plasmon detector and metal–oxide–semiconductor field-effect transistors," *IEEE Photon. J.*, vol. 5, no. 4, Aug. 2013, Art. no. 6800609.

[43] C. Hoessbacher, A. Josten, B. Baeuerle, Y. Fedoryshyn, H. Hettrich, Y. Salamin, W. Heni, C. Haffner, C. Kaiser, R. Schmid, D. L. Elder, D. Hillerkuss, M. Moller, L. R. Dalton, and J. Leuthold, "Plasmonic modulator with >170 GHz bandwidth demonstrated at 100 GBd NRZ," *Opt. Express*, vol. 25, no. 3, pp. 1762–1768, 2017.

[44] M. Ayata, Y. Fedoryshyn, W. Heni, B. Baeuerle, A. Josten, M. Zahner, U. Koch, Y. Salamin, C. Hoessbacher, C. Haffner, D. L. Elder, L. R. Dalton, and J. Leuthold, "High-speed plasmonic modulator in a single metal layer," *Science*, vol. 358, no. 6363, pp. 630–632, Nov. 2017.

[45] M. Ota, M. Fukuhara, A. Sumimura, M. Ito, T. Aihara, Y. Ishii, and M. Fukuda, "Dielectric-loaded surface plasmon polariton crossing waveguides using multimode interference," *Opt. Lett.*, vol. 40, no. 10, pp. 2269–2272, 2015.

[46] B. Steinberger, A. Hohenau, H. Ditlbacher, F. R. Aussenegg, A. Leitner, and J. R. Krenn, "Dielectric stripes on gold as surface plasmon waveguides: Bends and directional couplers," *Appl. Phys. Lett.*, vol. 91, no. 8, Aug. 2007, Art. no. 081111.

[47] Z. Zhang, M. Yako, K. Ju, N. Kawai, P. Chaisakul, T. Tsuchizawa, M. Hikita, K. Yamada, Y. Ishikawa, and K. Wada, "A new material platform of Si photonics for implementing architecture of dense wavelength division multiplexing on Si bulk wafer," *Sci. Technol. Adv. Mater.*, vol. 18, no. 1, pp. 283–293, Dec. 2017.

[48] A. Sumimura, M. Ota, K. Nakayama, M. Ito, Y. Ishii, and M. Fukuda, "Low-return-loss plasmonic multiplexer with tapered structure," *IEEE Photon. Technol. Lett.*, vol. 28, no. 21, pp. 2419–2422, Nov. 1, 2016.

[49] K. Nakayama, Y. Tonooka, M. Ota, Y. Ishii, and M. Fukuda, "Passive plasmonic demultiplexers using multimode interference," *J. Lightw. Technol.*, vol. 36, no. 10, pp. 1979–1984, May 15, 2018.

[50] M. Fukuhara, M. Ota, A. Takeda, T. Aihara, H. Sakai, Y. Ishii, and M. Fukuda, "Surface-plasmon waveguides as transmission lines for optical signal and electrical bias," *J. Lightw. Technol.*, vol. 32, no. 23, pp. 3888–3893, Dec. 1, 2014.

MITSUO FUKUDA (Member, IEEE) received the B.S. degree in electronic engineering from Ibaraki University, Ibaraki, Japan, in 1977, and the Ph.D. degree in physical electronics from the Tokyo Institute of Technology, Tokyo, Japan, in 1985. In 1977, he joined the NTT Electrical Communication Laboratories as a Research Engineer studying optical semiconductor devices used for various optical fiber communication systems. In 2004, he moved to the Toyohashi University of Technology as a Professor, where he studied plasmonic devices. In 2019, he reached mandatory retirement age and has since continuously been affiliated with the Toyohashi University of Technology as a Senior Researcher and Prof. Emeritus studying plasmonic devices.

SHINYA OKAHISA received the B.S. and M.S. degrees in electrical and electronic information engineering from the Toyohashi University of Technology, Toyohashi, Japan, in 2013 and 2015, respectively. He is currently affiliated with Pioneer Company.

YUTA TONOOKA received the B.S. and M.S. degrees in electrical and electronic information engineering from the Toyohashi University of Technology, Toyohashi, in Japan, 2017 and 2019, respectively. He is currently affiliated with Tokyo Electron Ltd.

MASASHI OTA (Member, IEEE) received the M.S. and Ph.D. degrees in electrical and electronic information engineering from the Toyohashi University of Technology, Toyohashi, Japan, in 2016 and 2019, respectively. He currently belongs to the NTT Science and Core Technology Laboratory Group.

TAKUMA AIHARA (Member, IEEE) received the M.S. and Ph.D. degrees in electrical and electronic information engineering from the Toyohashi University of Technology, Toyohashi, Japan, 2012 and 2015, respectively. He currently belongs to the NTT Science and Core Technology Laboratory Group.

YASUHIKO ISHIKAWA (Member, IEEE) received the B.S., M.S., and Ph.D. degrees from Hokkaido University, Japan, in 1993, 1995, and 1998, respectively. Since 2017, he has been a Professor with the Department of Electrical and Electronic Information Engineering, Toyohashi University of Technology, Toyohashi, Japan. Before joining the Toyohashi University of Technology, he was an Associate Professor with The University of Tokyo, Tokyo, Japan. His research interest includes Si-based photonic devices and their applications to communication and sensing systems.